Supporting Material for Potassium buffering in the neurovascular unit: Models and sensitivity analysis

Alexandra Witthoft,[†] Jessica A. Filosa,[‡] and George Em Karniadakis[*§]

[†]School of Engineering, Brown University, Providence, RI 02912
[‡]Department of Physiology, Georgia Regents University, Augusta, GA 30912
[§]Division of Applied Mathematics, Brown University, Providence, RI 02912

[*]Correspondence: Tel.: +00-1-401-8631217. E-mail: George_Karniadakis@brown.edu

S1 Detailed Model Equations

S1.1 Synaptic Space, Ω_S

When neurons are activated, they release K^+ and glutamate into the synaptic space (see Fig. 1). The governing equation for the potassium in the synaptic space is

$$\frac{\mathrm{d}[\mathrm{K}^+]_S}{\mathrm{d}t} = J_{K_s} - (J_{NaK,K} + J_{NKCC} + J_{Kir,AS})\frac{1}{VR_{sa}} - Rdc_{\mathrm{K}^+,S}([\mathrm{K}^+]_S - [\mathrm{K}^+]_{S,0}), \tag{S1}$$

where J_{K_S} is a smooth pulse approximation of potassium release from active neurons; J_{NKCC} is the astrocyte potassium uptake through the Na-K-Cl cotransport (Eq. (S7), below), $J_{NaK,K}$ is the astrocytic K^+ uptake through the Na-K pump (Eq. (S5), below), and VR_{sa} is the volume ratio of synaptic space to astrocyte intracellular space. $J_{Kir,AS} = I_{Kir,AS}/(C_{ast}\gamma)$ is the astrocytic $\mathrm{Kir_{AS}}$ flux into the perisynaptic processes (Eq. (S9), below), where C_{ast} is the astrocyte cell capacitance, and γ is a scaling factor for relating the net movement of ion fluxes to the membrane potential ([1]). $[\mathrm{K}^+]_{S,0}$ is the baseline K^+ concentration, and $Rdc_{\mathrm{K}^+,S}$ is the decay rate.

The synaptic glutamate release is assumed to be a smooth pulse, and the ratio of active to total G-protein due to mGluR binding on the astrocyte endfoot is given by

$$G^* = \frac{\rho + \delta}{K_G + \rho + \delta}, \tag{S2}$$

where $\rho = [Glu]/(K_{Glu} + [Glu])$ is the ratio of bound to unbound receptors, and δ is the ratio of the activities of bound and unbound receptors, which allows for background activity in the absence of a stimulus ([2]).

S1.2 Astrocytic Intracellular Space, Ω_{Astr}

Two astrocyte activities occur simultaneously in response to the extracellular K^+ and glutamate:

(1) The glutamate binds to receptors on the astrocyte perisynaptic process, and IP_3 production occurs inside the cell wall, causing release of intracellular Ca^{2+}, which both inhibits TRPV4 channels and triggers EET production. Both Ca^{2+} and EET activate the astrocytic BK channels, which release K^+ into the perivascular space. In addition, vessel dilation (strain, ϵ) activates the TRPV4 channels, allowing an influx of Ca^{2+} into the astrocyte.

(2) Happening concurrently, the extracellular K^+ increase leads to K^+ influx through astrocyte Na-K pump and perisynaptic $\mathrm{Kir_{AS}}$ channels, resulting in a membrane depolarization and a rise in astrocytic intracellular K^+, along with a decrease in intracellular Na^+. The NKCC influx increases with decreasing intracellular Na^+, K^+, and Cl^-; thus, the cotransport depends on the competition between K^+ influx and Na^+ outflux. This activates outward K^+ current through the perivascular endfoot $\mathrm{Kir_{AV}}$ channels, which release K^+ at the perivascular interface.

Perisynaptic processes (1)

The IP_3 production in the astrocyte is based on the model by [2] as modified by [3]:

$$\frac{\mathrm{d}[\mathrm{IP}_3]}{\mathrm{d}t} = r_h^* G^* - k_{deg}[\mathrm{IP}_3], \tag{S3}$$

where r_h^* is the IP_3 production rate, and k_{deg} is the degradation rate.

Perisynaptic processes (2)

The electrical current through the Na-K pump is carried by both Na^+ and K^+ ions, thus we treat it as the sum of these components:

$$I_{NaK} = I_{NaK,K} + I_{NaK,Na}, \tag{S4}$$

where the potassium current is carried by an influx of K^+ ions which is described by the Na-K potassium flux from [3]:

$$J_{NaK,K} = J_{NaK,max}\frac{[\mathrm{K}^+]_S}{[\mathrm{K}^+]_S + KKo_a}\frac{[\mathrm{Na}^+]^{1.5}}{[\mathrm{Na}^+]^{1.5} + KNa_i^{1.5}}, \tag{S5}$$

where $J_{NaK,max}$ is the maximum K^+ flux through the channel; the potassium concentration in the synaptic space is $[\mathrm{K}^+]_S$, and KKo_a is the threshold value for $[\mathrm{K}^+]_S$. $[\mathrm{Na}^+]$ is the intracellular sodium concentration, and KNa_i is the threshold value. VR_{sa} is the volume ratio of the astrocyte intracellular space to the synaptic space. All astrocyte

cation currents, I_{i^+}, are related to the corresponding cation concentration flux, J_{i+}, as $I_{i^+} = -J_{i^+}C_{ast}\gamma$, where C_{ast} is the astrocyte cell capacitance, and γ is a scaling factor for relating the net movement of ion fluxes to the membrane potential [1]. (For anion flux, the factor of -1 is removed). Thus, the potassium current in the astrocyte due to Na/K is $I_{NaK,K} = -J_{NaK,K}C_{ast}\gamma$. The Na-K pump exchanges 3 sodium ions for every 2 potassium ions, so the Na^+ current is

$$I_{NaK,Na} = -\frac{3}{2}I_{NaK,K}. \tag{S6}$$

The NKCC is electrically silent because its total uptake comprises two positive charges (an Na^+ and K^+ ion) for every two negative charges (two Cl^- ions): a net charge of zero. The equation for the NKCC flux is adapted from the model developed by [4]:

$$J_{NKCC} = J_{NKCC,max}\log\left[\frac{[K^+]_S}{[K^+]_A}\frac{[Na^+]_S}{[Na^+]_A}\left(\frac{[Cl^-]_S}{[Cl^-]_A}\right)^2\right], \tag{S7}$$

where the subscripts A and S indicate concentrations in the astrocyte and synaptic space, respectively, and $J_{NKCC,max}$ is the scaling factor that determines the amplitude of the pump flux. The potassium and sodium fluxes through the cotransport are $J_K = J_{NKCC}$ and $J_{Na} = J_{NKCC}$, because the cotransport mechanism carries one K^+ ion for every Na^+ ion. Because our model does not include mechanisms that interact with chloride dynamics and because the astrocytic Cl^- and Na^+ concentrations are roughly the same at baseline and active states ([4]), we add the simplification that $[Cl^-]_A = [Na^+]_A$. In addition, we also assume a constant value for the extracellular Cl^- and Na^+, $[Cl^-]_S$ and $[Na^+]_S$, respectively.

The intracellular Na^+ concentration obeys

$$\frac{\mathrm{d}[Na^+]_A}{\mathrm{d}t} = J_{NaK,Na} + J_{NKCC}, \tag{S8}$$

where $J_{NaK,Na} = -I_{NaK,Na}/(C_{ast}\gamma)$.

Astrocytes in the cortex have homomeric Kir4.1 channels and heteromeric Kir4.1/5.1 channels; both are present in the perisynaptic processes, but the endfeet express only the heteromer ([5]). Also, it is worth noting, astrocytes in thalamus and hippocampus, where there are abundant synapses, express predominantly the Kir4.1 homomer ([5]). The heteromer has a higher single channel conductance, but few data exist on the Kir channel densities along astrocyte bodies except in the retina ([6, 7]), where astrocyte function is unique and highly specialized. Therefore, we estimate the relative whole-cell Kir conductances at the endfeet and processes by adjusting for the appropriate K^+ fluxes and astrocyte membrane potential during simulation. The main difference between the Kir4.1 homomer and Kir 4.1/4.5 heteromer is the difference in their response to pH ([5]). At the moment, the model does not include a description of astrocytic pH, but when this is added at future time, it will be important to consider its nonuniform inhibitory effects on the process and endfeet Kir channels.

The current through the perisynaptic Kir_{AS} channels is

$$I_{Kir,AS} = g_{Kir,AS}(V_A - V_{Kir,AS}), \tag{S9}$$

where AS stands for the Astrocyte-Synapse interface. The channel conductance, $g_{Kir,AS}$ is calibrated to the the glial Kir4.1 data from [8]; the reversal potential, $V_{Kir,AS}$, is the Nernst potential for potassium. The conductance is defined as

$$g_{Kir,AS} = g_{Kir,S}\sqrt{[K^+]_S}, \tag{S10}$$

where $[K^+]_S$ is the potassium concentration in the synaptic space in mM, and $g_{Kir,S}$ is a proportionality constant. The reversal potential is

$$V_{Kir,AS} = E_{Kir,proc}\log\frac{[K^+]_S}{[K^+]_A}, \tag{S11}$$

where $E_{Kir,proc}$ is the Nernst constant for the astrocyte process Kir channels (about 25 mV [9]).

Astrocyte soma (1)

The astrocytic intracellular $[Ca^{2+}]$ obeys

$$\frac{\mathrm{d}[Ca^{2+}]}{\mathrm{d}t} = \beta(J_{IP_3} - J_{pump} + J_{leak}) + J_{TRP}, \tag{S12}$$

where the first three terms are Ca^{2+} fluxes from the ER into the cytosol (Eqs. (S13) – (S16) below); β is the factor describing Ca^{2+} buffering, and the Ca^{2+} influx through the TRPV4 channels is $J_{TRP} = -(1/2)I_{TRP}/(C_{ast}\gamma)$ (see Eq. (S26), below).

The calcium stores in the ER have three mechanisms for calcium transport: (1) IP_3R receptors on the ER bind to intracellular IP_3, initiating Ca^{2+} outflux from the ER, J_{IP_3} into the intracellular space; (2) a pump uptakes Ca^{2+} from the cytosol into the ER, J_{pump}, and (3) a leak flux J_{leak} from the ER into the intracellular space ([2]). The IP_3-dependent current is

$$J_{IP_3} = J_{max}\left[\left(\frac{[IP_3]}{[IP_3]+K_I}\right)\left(\frac{[Ca^{2+}]}{[Ca^{2+}]+K_{act}}\right)h\right]^3\left(1-\frac{[Ca^{2+}]}{[Ca^{2+}]_{ER}}\right), \tag{S13}$$

where J_{max} is the maximum rate; K_I is the dissociation constant for IP_3R binding; K_{act} is the dissociation constant for Ca^{2+} binding to an activation site on the IP_3R, and $[Ca^{2+}]_{ER}$ is the Ca^{2+} concentration in the ER. The gating variable h is governed by

$$\frac{dh}{dt} = k_{on}[K_{inh} - ([Ca^{2+}] + K_{inh})h], \tag{S14}$$

where k_{on} and K_{inh} are the Ca^{2+} binding rate and dissociation constant, respectively, at the inhibitory site on the IP_3R. The pump flux is

$$J_{pump} = V_{max}\frac{[Ca^{2+}]^2}{[Ca^{2+}]^2 + K_p^2}, \tag{S15}$$

where V_{max} is the maximum pump rate, and K_p is the pump constant. The leak channel flux is

$$J_{leak} = P_L\left(1-\frac{[Ca^{2+}]}{[Ca^{2+}]_{ER}}\right), \tag{S16}$$

where P_L is determined by the steady-state flux balance.

The rise in intracellular Ca^{2+} in the astrocyte leads to EET production inside the cell. The EET production is governed by

$$\frac{d[EET]}{dt} = V_{EET}([Ca^{2+}] - [Ca^{2+}]_{min}) - k_{EET}[EET], \tag{S17}$$

where V_{EET} is the EET production rate; $[Ca^{2+}]_{min}$ is the minimum $[Ca^{2+}]$ required for EET production, and k_{EET} is the EET decay rate. Following [3], we assume that EET acts only on the astrocyte BK channels in the perivascular endfoot, rather than acting directly on the arteriole SMC as in [2].

Astrocyte soma (2)

The intracellular K^+ concentration, $[K^+]_A$, rises due to influx through Kir_{AS} and Na-K pump:

$$\frac{d[K^+]_A}{dt} = J_{NaK,K} + J_{NKCC} + J_{Kir,AS} + J_{BK} + J_{Kir,AV} - Rdc_{K^+,A}([K^+]_A - [K^+]_{A,0}), \tag{S18}$$

where any potassium flux J is related to the corresponding electrical current I such that $J_i = -I_i/(C_{ast}\gamma)$ (for $i = [(NaK,K),(Kir,AS),BK,(Kir,AV)]$; $[K^+]_{A,0}$ is the baseline K^+ concentration, and $Rdc_{K^+,A}$ is the decay rate.

We assume in this model that the astrocyte membrane potential is uniform across the entire cell; it is likely that this is not the case, as similar membrane structures (e.g. neuronal dendritic trees) are highly lossy. However, for simplicity, we consider the astrocyte as a single electrical compartment in which the membrane potential obeys

$$\frac{dV_A}{dt} = \frac{1}{C_{ast}}(-I_{NaK} - I_{Kir,AS} - I_{BK} - I_{TRP} - I_{Kir,AV} - I_{leak}), \tag{S19}$$

where C_{ast} is the astrocyte cell capacitance; I_{NaK} is the Na-K pump current (Eq. (S4)), the Kir_{AS} and Kir_{AV} channel currents at the processes and endfeet are $I_{Kir,AS}$ and I_{Kir_AV} (Eqs. (S9) and (S30)) respectively; the BK current is I_{BK} (Eq. (S21), below), and the TRP current is I_{TRP} (Eq. (S26), below). The leak current, I_{leak} is

$$I_{leak} = g_{leak}(V_A - v_{leak}), \tag{S20}$$

where g_{leak} and v_{leak} are the leak conductance and reversal potential, respectively.

Perivascular endfeet (1)

Astrocytic BK channels, which occur on the perivascular endfeet, are affected by both EET and Ca^{2+}, as described by [3]:

$$I_{BK} = g_{BK} n_{BK} (V_A - v_{BK}), \tag{S21}$$

where g_{BK} is the channel conductance; v_{BK} is the reversal potential, and n_{BK} is governed by

$$\frac{\mathrm{d}n_{BK}}{\mathrm{d}t} = \phi_{BK}(n_{BK\infty} - n_{BK}), \tag{S22}$$

with

$$\phi_{BK} = \psi_{BK} \cosh\left(\frac{V_A - v_{3,BK}}{2v_{4,BK}}\right), \tag{S23}$$

$$n_{\infty,BK} = 0.5\left(1 + \tanh\left(\frac{V_A + EET_{shift}[\mathrm{EET}] - v_{3,BK}}{v_{4,BK}}\right)\right). \tag{S24}$$

Also $v_{3,BK}$ is the potential associated with 1/2 open probability, which depends on $[Ca^{2+}]$:

$$v_{3,BK} = -\frac{v_{5,BK}}{2} \tanh\left(\frac{[Ca^{2+}] - Ca_{3,BK}}{Ca_{4,BK}}\right) + v_{6,BK}, \tag{S25}$$

where $v_{4,BK}$, $v_{5,BK}$, $v_{6,BK}$, $Ca_{3,BK}$, $Ca_{4,BK}$, and ψ_{BK} are constants, and EET_{shift} determines the EET-dependent shift in the channel open probability.

In the astrocyte perivascular endfoot, the mechanosensitive TRPV4 channels allow calcium influx from extracellular space, J_{TRPV}, in response to arteriolar dilations and constrictions which stretch the enclosing endfoot membrane. These channels are also inhibited by astrocytic intracellular Ca^{2+} increases. The electrical current through the channel is

$$I_{TRP} = g_{TRP} s (V_A - v_{TRP}), \tag{S26}$$

where g_{TRP} is the maximum channel conductance; v_{TRP} is the channel reversal potential, and V_A is the membrane potential (see Eq. (S19) below). The calcium ion flux through the channel is given by $J_{TRP} = -(1/2)I_{TRP}/(C_{ast}\gamma)$. There is a factor of -1 because J_{TRP} is a flux of positive ions, whereas electrical current, I_{TRP}, always describes the motion of negative charges (an outflux of electrons being equivalent to an influx of positive ions). The factor of 1/2 is there because there are two positive charges for every one calcium ion.

The TRPV4 channel current is activated by mechanical stretches, and, after activation stops, experiences a slow decay in the absence of extracellular Ca^{2+}, and a fast decay in the presence of high extracellular Ca^{2+} ([10, 11]). Thus, we model the open probability as an ODE that decays to its variable steady state, s_∞ (Eq. (S28), below), according to

$$\frac{\mathrm{d}s}{\mathrm{d}t} = \frac{1}{\tau_{Ca}([Ca^{2+}]_P)}(s_\infty - s), \tag{S27}$$

where the Ca^{2+}-dependent time constant $\tau_{Ca}([Ca^{2+}]_P) = \tau_{TRP}/[Ca^{2+}]_P$, where $[Ca^{2+}]_P$ is the perivascular Ca^{2+} concentration (Eq. (S34), below) expressed in μM, and s_∞ is the strain- and Ca^{2+}-dependent steady-state channel open probability: We model the steady-state TRPV4 channel open probability, s_∞, by the Boltzmann equation [12, 1]:

$$s_\infty = \left(\frac{1}{1 + e^{-(\epsilon - \epsilon_{1/2})/\kappa}}\right)\left[\frac{1}{1 + H_{Ca}}\left(H_{Ca} + \tanh\left(\frac{V_A - v_{1,TRP}}{v_{2,TRP}}\right)\right)\right]. \tag{S28}$$

The first term $1/(1 + e^{-(\epsilon - \epsilon_{1/2})/\kappa})$ describes the material strain gating, adapted from [1]. The strain on the perivascular endfoot, ϵ, is taken to be the same as the local radial strain on the arteriole $\epsilon = (r - r_0)/r_0$ (see Eq. (S50), below), while $\epsilon_{1/2}$ is the strain required for half-activation. The second term describes the voltage gating and Ca^{2+} inhibitory behavior, based on the experimental results from [11] and [13]. The parameters $v_{1,TRP}$ and $v_{2,TRP}$ are the membrane potential required for half-activation and the steepness of the voltage gating curve, respectively. The inhibitory term, H_{Ca}, is

$$H_{Ca} = \left(\frac{[Ca^{2+}]}{\gamma_{Ca_i}} + \frac{[Ca^{2+}]_P}{\gamma_{Ca_e}}\right), \tag{S29}$$

where $[Ca^{2+}]$ is the astrocytic intracellular Ca^{2+} concentration (Eq. (S12)); $[Ca^{2+}]_P$ is the perivascular Ca^{2+} concentration (Eq. (S34), below), and γ_{Ca_i} and γ_{Ca_e} are constants associated with intra- and extracellular Ca^{2+}, respectively.

We point out that this TRPV4 model is a simplified description of the true TRPV4 channel, which has a highly complex and diverse range of gating properties. For instance, it has been reported that at low levels, intracellular calcium potentiates channel activity, rather than inhibiting it [14]. During a neuronal stimulus, this might affect the initial behavior of the TRPV4 channel during the brief period when the astrocyte intracellular Ca^{2+} is still low. However, both the astrocyte intracellular Ca^{2+} dynamics and the TRPV4 gating properties are not yet known with enough fine precision for a more detailed TRPV4 model to be useful. TRPV4 channels have been observed to respond to a variety of additional variables including temperature and diffusibles such as EET and IP_3 [15, 10, 13].

Thus, this model is a simplified description of TRPV4, focusing mainly on its mechanosensitive properties, as this is sufficient to capture the astrocyte response to vessel movement (refer to [16]), but additional gating properties can be added to the model in the future as more data become available.

Perivascular endfeet (2)

At the perivascular endfoot, the Kir_{AV} current is

$$I_{Kir,AV} = g_{Kir,AV}(V_A - V_{Kir,AV}), \tag{S30}$$

where AV stands for the Astrocyte-Vessel interface. The conductance and reversal potential, $g_{Kir,AV}$ and $V_{Kir,AV}$ are shown below:

$$g_{Kir,AV} = g_{Kir,V}\sqrt{[\text{K}^+]_{PV}}, \tag{S31}$$

where $[\text{K}^+]_{PV}$ is the potassium concentration in the perivascular space in mM, and $g_{Kir,V}$ is a proportionality constant. The reversal potential is again the Nernst potential, but because the channel is located at the perivascular endfoot, $V_{Kir,AV}$ depends on the perivascular K^+ concentration instead of the synaptic space concentration:

$$V_{Kir,AV} = E_{Kir,endfoot}\log\frac{[\text{K}^+]_{PV}}{[\text{K}^+]_A}. \tag{S32}$$

S1.3 Perivascular Space, Ω_P

The potassium accumulates in the perivascular space due to outflow from astrocytic BK and Kir_{AV} channels and arteriolar smooth muscle cell Kir_{SMC} channels. The equation governing perivascular K^+ is

$$\frac{\text{d}[\text{K}^+]_{PV}}{\text{d}t} = -\frac{J_{BK} + J_{Kir,AV}}{VR_{pa}} - \frac{J_{Kir,SMC}}{VR_{ps}} - R_{dc}([\text{K}^+]_{PV} - [\text{K}^+]_{P,0}), \tag{S33}$$

where VR_{pa} and VR_{ps} are the volume ratios of perivascular space to astrocyte and SMC, respectively, and $[\text{K}^+]_{P,0}$ is the resting state equilibrium K^+ concentration in the perivascular space. R_{dc} is the rate at which perivascular K^+ concentration decays to its baseline state due to a combination of mechanisms including uptake in background cellular activity and diffusion through the extracellular space. The potassium flow from the astrocyte and SMC are $J_{BK} + J_{Kir,AV}$ and $J_{Kir,SMC}$, respectively, given as $J_{BK} = -I_{BK}/(C_{ast}\gamma)$, $J_{Kir,AV} = -I_{Kir,AV}/(C_{ast}\gamma)$, and $J_{Kir,SMC} = -I_{Kir,SMC}/(C_{SMC}\gamma)$ (Eqs. (S21), (S30) and (S36), below), where C_{SMC} is the SMC capacitance.

The perivascular Ca^{2+} concentration obeys

$$\frac{\text{d}[\text{Ca}^{2+}]_P}{\text{d}t} = -J_{Ca} - J_{TRPV} - Ca_{dc}([\text{Ca}^{2+}]_P - [\text{Ca}^{2+}]_{P,0}), \tag{S34}$$

where J_{Ca} is the calcium current from the arteriole SMC (see Eq. (S47) below), and Ca_{dc} is the decay rate of perivascular Ca^{2+} concentration (similar to R_{dc}).

S1.4 Arteriole Smooth Muscle Cell Intracellular Space, Ω_{SMC}

The arteriole tone depends on the level of intracellular Ca^{2+} in the SMC (see Fig. 1) When the arteriolar Kir_{SMC} channels are activated due to perivascular K^+, the SMC membrane potential experiences a hyperpolarization, which closes Ca^{2+} channels. The decreased Ca^{2+} level in the SMC intracellular space results in a dilation, corresponding to strain, ϵ, which then activates the astrocytic TRPV4 channels.

The equations for the SMC dynamics are adopted from [17] except that the membrane potential is modified to include the Kir_{SMC} current (Eq. (S36)) following [3]:

$$\frac{\text{d}V_m}{\text{d}t} = \frac{1}{C_{SMC}}(-I_L - I_K - I_{Ca} - I_{Kir,SMC}), \tag{S35}$$

where C_{SMC} is the cell capacitance, and I_L, I_K, and I_{Ca} are the leak, K^+ channel potassium, and calcium currents, respectively (Eqs. (S42) – (S49), below).

The vascular SMC model from [17] describes vasomotion as a result of pressure-sensitive Ca^{2+} ion channel activity in the SMC (see Eqs. (S48) and (S49), below). Other models assume that vasomotion is also affected by endothelial cell activity ([1, 3]). Both the SMC and endothelial cells are likely to have a contribution to vasomotion. However, there have been observations of vasomotion in arterioles in which the endothelium was removed ([18]), indicating that the endothelium is not required for vasomotion, even if it can have an effect. Thus, for simplicity, the role of endothelial cells is not addressed here, but can be added to the model at a later time.

The potassium buildup in the perivascular space activates the arteriolar Kir_{SMC} channels according to ([3])

$$I_{Kir,SMC} = g_{Kir,SMC} k (V_m - v_{Kir,SMC}), \tag{S36}$$

where the channel conductance, $g_{Kir,SMC}$, reversal potential, $v_{Kir,SMC}$, and open probability, k, all depend on the perivascular K^+ concentration:

$$g_{Kir,SMC} = g_{Kir,0} \sqrt{[K^+]_{PV}}, \tag{S37}$$

where $[K^+]_{PV}$ is in units of mM, and $g_{Kir,0}$ is the conductance when the perivascular K^+ concentration is 1 mM;

$$v_{Kir,SMC} = v_{Kir,1} \log [K^+]_{PV} - v_{Kir,2}, \tag{S38}$$

where $[K^+]_{PV}$ is again in units of mM, and $v_{Kir,1}$ and $v_{Kir,2}$ are constants, and

$$\frac{dk}{dt} = \frac{1}{\tau_k}(k_\infty - k), \tag{S39}$$

where $\tau_k = 1/(\alpha_k + \beta_k)$, and $k_\infty = \alpha_k/(\alpha_k + \beta_k)$, in which

$$\alpha_k = \frac{\alpha_{Kir}}{1 + \exp(\frac{V_m - v_{Kir} + a_{v_1}}{a_{v_2}})} \tag{S40}$$

$$\beta_k = \beta_{Kir} \exp(b_{v_2}(V_m - v_{Kir} + b_{v_1}), \tag{S41}$$

where α_{Kir}, β_{Kir}, a_{v_1}, a_{v_2}, b_{v_1}, and b_{v_2} are constants ([3]). The SMC membrane potential is V_m (Eq. (S35)).

The leak current is simply $I_L = g_L(V_m - v_L)$, where g_L is the leak conductance, and v_L is the leak reversal potential. The K^+ channel current is

$$I_K = -g_K n (V_m - v_K), \tag{S42}$$

where g_K and v_K are the channel conductance and reversal potential, respectively. The fraction of K^+ channel open states, n is described by

$$\frac{dn}{dt} = \lambda_n (n_\infty - n), \tag{S43}$$

with

$$n_\infty = 0.5 \left(1 + \tanh \frac{V_m - v_3}{v_4}\right), \tag{S44}$$

and

$$\lambda_n = \phi_n \cosh \frac{V_m - v_3}{2 v_4}, \tag{S45}$$

where v_4 is the spread of the open state distribution with respect to voltage, and v_3 is the voltage associated with the opening of half the population, and is dependent on the Ca^{2+} concentration in the SMC:

$$v_3 = -\frac{v_5}{2} \tanh \frac{[Ca^{2+}]_{SMC} - Ca_3}{Ca_4} + v_6. \tag{S46}$$

The parameters Ca_3 and Ca_4 affect the shift and spread of the distribution, respectively, of v_3 with respect to Ca^{2+}, and v_5, v_6 are constants. The Ca^{2+} channel current is

$$I_{Ca} = g_{Ca} m_\infty (V_m - v_{Ca}), \tag{S47}$$

where g_{Ca} and v_{Ca} are the channel conductance and reversal potential, respectively. Since *fast kinetics* are assumed for the Ca^{2+} channel, the distribution of open channel states is equal to the equilibrium distribution

$$m_\infty = 0.5 \left(1 + \tanh \frac{V_m - v_1}{v_2}\right), \tag{S48}$$

with v_1 and v_2 having the same effect as Ca_3 and Ca_4 in Eq. (S46) and v_3 and v_4 in Eq. (S44). Note that in this case, v_1 is a variable that depends on the transmural pressure. We represent the relationship using this linear approximation of the data from [17]:

$$v_1 = -17.4 - 12\Delta P/200, \tag{S49}$$

where ΔP is in units of mmHg, and v_1 is in mV. For our model, we chose a value of 60 mmHg for ΔP, which we found to be consistent with experimental observations (e.g. Figure 5 in [19]) for arterioles around 50 μm in diameter, the size used in our simulations.

The SMC myogenic contractile behavior, which constricts the vessel, depends on the Ca^{2+} concentration in the SMC. The vessel circumference, x, is described by

$$\frac{dx}{dt} = \frac{1}{\tau}(f_{\Delta P} - f_x - f_u), \tag{S50}$$

where the radius r comes from $x = 2\pi r$; τ is the time constant, and $f_{\Delta P}$ f_x f_u are the forces due to transmural pressure, viscoelasticity of the material, and myogenic response, respectively. The myogenic force, f_u depends on the SMC Ca^{2+} concentration, which changes based on the Ca^{2+} ion channel current. These forces are discussed in detail in [17].

S2 Additional Sensitivity Analysis Results

In this section we analyze the system sensitivity to all 55 parameters using the ANOVA functional decomposition and stochastic collocation [20, 21, 22] in which two parameters at a time are varied simultaneously. (Contrast with Section 4, in which we performed a global sensitivity analysis of a subset of eight key parameters, all of which were varied simultaneously.)

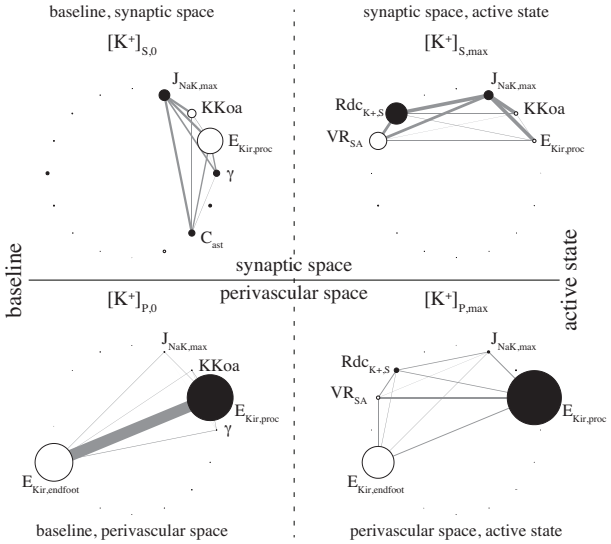

Figure S1: *Sensitivity of baseline and maximum extracellular potassium.* Small circles indicate single parameter sensitivity equal to diameter of the circle; style indicates that increased parameter magnitude will increases (*open*) or decrease (*solid*) the value of the metric: (*top left and right*) extracellular K^+ in synaptic space at baseline, $[K^+]_{S,0}$, and active state, $[K^+]_{S,max}$; (*bottom left and right*) extracellular K^+ in perivascular space at baseline, $[K^+]_{P,0}$, and active state, $[K^+]_{P,max}$, respectively. Thicknesses of grey lines indicate sensitivity of two-parameter interaction pair.

Fig. S1 shows four quadrants, each with sensitivity results for extracellular potassium concentration: The top row is the sensitivity of potassium concentration in the synaptic space, while the bottom row is the potassium concentration in the perivascular space; the left column is the baseline level, and the right column is the maximum concentration when the system is in the active state[1].

In each quadrant, consider all 55 the model parameters are arranged in a large ring, but to make the diagram easier to see, we have only labeled the parameters we have determined to be most sensitive. The data in this figure are visualized the same way as in Figure 5 from Section 4.

In the top left quadrant, the most sensitive parameters for the synaptic space baseline K^+ level are the following: $J_{NaK,max}$; $KKoa$, the threshold value of extracellular K^+ for the Na-K pump in the astrocyte process; $E_{Kir,proc}$; γ, the conversion factor relating flux of ionic concentration to electric current in the astrocyte membrane; and C_{ast}, the capacitance of the astrocytic membrane. The most sensitive parameter is $E_{Kir,proc}$, which implies that the astrocyte Kir_{AS} channels are the most important mechanism setting the baseline level of synaptic K^+. Likewise, in the lower left quadrant, the baseline perivascular K^+ level is most sensitive to the astrocyte endfoot Kir_{AV} and

[1] meaning that there is synaptic activity, which we model as a release of potassium and glutamate in the synaptic space near the synapse-adjacent astrocyte process

process Kir_{AS} channel reversal potentials ($E_{Kir,proc}$ and $E_{Kir,endfoot}$, respectively). We note that these findings are limited to an isolated astrocyte; intercellular inputs from adjacent astrocytes via gap junctions and diffusible biochemical messengers may have a profound impact impact on the results if they are included in the model.

It is worthwhile to consider baseline K^+ sensitivities (the left-hand side, top and bottom quadrants) together: note that the synaptic space and perivascular space baseline K^+ levels are both sensitive to several of the same parameters: $J_{NaK,max}$, $KKoa$, $E_{Kir,proc}$, and γ. This reveals an inherent model assumption about the connectivity of the two ends of the astrocyte, which is a possible limitation of the model. In the future, it may be necessary to upgrade the model into a multi-compartment model in which some loss exists in the propagation of ions and electric signals from one end of the cell to the other. Gap junctions between neighboring astrocytes may also need to be added to the model in the future as these would contribute to the distribution of ions throughout the glial network. The same is evident in comparing the active state K^+ in the synaptic and perivascular regions (right-hand side, top and bottom quadrants). Again, out of all 55 parameters in the model, the maximum K^+ level in the synaptic and perivascular spaces share four out of five of their top most sensitive parameters: VR_{SA}, $Rdc_{K^+,S}$, $J_{NaK,max}$, and $E_{Kir,proc}$.

S3 Simulation Parameters

Table S1: Ω_s Synaptic Space

Ω_s Synaptic Space		Description	Source
$Rdc_{\text{K}^+,S}$	0.07 s^{-1}	K^+ decay rate in synaptic space	estimation
VR_{sa}	3	volume ratio of synaptic space to astrocyte intracellular space	estimate – [3]
$[\text{Na}^+]_S$	169 mM	synaptic space Na^+ concentration	estimate – [4]

Table S2: Ω_{astr} Astrocytic Intracellular Space

Ω_{astr} Astrocytic Intracellular Space		Description	Source
astrocyte perisynaptic process			
$E_{Kir,proc}$	26.797 mV	Nernst constant for perisynaptic process Kir_{AS} channels	estimate – [9]
$g_{Kir,S}$	144 pS	proportionality constant for perisynaptic process Kir_{AS} conductance	[5]
KNa_i	1 mM	intracellular Na^+ threshold value for Na-K pump	estimation
KKo_a	16 mM		estimation
$J_{NaK_{max}}$	1.4593 mM/sec	maximum Na-K pump rate	estimation
$J_{NKCC,max}$	0.07557 mM/sec	NKCC pump rate	estimation
δ	0.001235		[3]
K_G	8.82		[3]
astrocyte soma			
r_h	4.8 μM		[3]
k_{deg}	1.25 s^{-1}		[3]
β_{cyt}	0.0244		[3]
K_{inh}	0.1 μM		[2]
k_{on}	2 $\mu\text{M}^{-1}\text{s}^{-1}$		[2]
J_{max}	2880 μMs^{-1}		[2]
K_I	0.03 μM		[2]
K_{act}	0.17 μM		[2]
V_{max}	20 μMs^{-1}		[2]
k_{pump}	0.192 μM		estimation
P_L	5.2 μMs^{-1}		[3]
$[\text{Ca}^{2+}]_{min}$	0.1 μM	minimum intracellular Ca^{2+} required for EET production	[3]
V_{EET}	72 s^{-1}		[3]
k_{EET}	7.1 s^{-1}		[3]
C_{ast}	40 pF	astrocyte membrane capacitance	[3]
g_{leak}	3.7 pS	leak channel conductance	estimation

v_{leak}	-40 mV	leak channel reversal potential	estimation
γ	834.3 mVμM^{-1}	scaling factor relating ion flux to membrane potential	[23]
$Rdc_{\mathrm{K}^+,A}$ *perivascular endfoot*	0.15 s^{-1}	astrocyte intracellular K^+ decay rate	estimation
$g_{Kir,V}$	25 pS	proportionality constant for endfoot $\mathrm{Kir_{AV}}$ conductance	[5]
$E_{Kir,endfoot}$	31.147 mV	Nernst constant for endfoot $\mathrm{Kir_{AV}}$ channels	estimate – [9]
g_{BK}	200 pS	BK channel conductance	[24]
v_{BK}	-80 mV	BK channel reversal potential	[24]
EET_{shift}	2 mVμM^{-1}		[3]
$v_{4,BK}$	14.5 mV		[3]
$v_{5,BK}$	8 mV		[3]
$v_{6,BK}$	-13 mV		[3]
ψ_n	2.664 s^{-1}		[3]
$Ca_{3,BK}$	400 nM		[3]
$Ca_{4,BK}$	150 nM		[3]
g_{TRPV}	50 pS	TRPV4 channel conductance	[25]
v_{TRPV}	6 mV	TRPV4 channel reversal potential	[26]
κ	0.1		fit to [27]
$v_{1,TRPV}$	120 mV		fit to [10, 11]
$v_{2,TRPV}$	13 mV		fit to [10, 11]
$\epsilon_{1/2}$	0.1		fit to [27]
γ_{Ca_i}	0.01 μM		fit to [11]
γ_{Ca_e}	0.2 mM		fit to [10]
τ_{TRPV}	0.9 s^{-1}		fit to [27, 11]

Table S3: Ω_P Perivascular Space

Ω_P Perivascular Space		Description	Source
$[\mathrm{Ca}^{2+}]_{P,0}$	5 μM		estimation
VR_{pa}	0.04		estimate – [3]
VR_{ps}	0.1		estimate – [3]
R_{dc}	0.2 s^{-1}	K^+ decay rate in perivascular space	estimate – [3]
$[\mathrm{K}^+]_{P,0}$	1 mM	minimum K^+ concentration in perivascular space	estimate – [3]

Table S4: Ω_{SMC} $\mathrm{Kir_{SMC}}$ Channels in Vascular Smooth Muscle Cell

Ω_{SMC} Vascular Smooth Muscle Cell Space		Description	Source
$v_{KIR,1}$	48.445 mV	factor relating $\mathrm{Kir_{SMC}}$ reversal potential to extracellular K^+	estimate – [16, 3]
$v_{KIR,2}$	116.09 mV	minimum $\mathrm{Kir_{SMC}}$ reversal potential (at low extracellular K^+)	estimate – [16, 3]
$g_{KIR,0}$	120 pS	factor relating $\mathrm{Kir_{SMC}}$ conductance to extracellular K^+	estimate – [3]
α_{KIR}	1020 sec	parameter for $\mathrm{Kir_{SMC}}$ opening rate, α_k	[3]
a_{v_1}	18 mV	parameter for $\mathrm{Kir_{SMC}}$ opening rate, α_k	[3]
a_{v_2}	6.8 mV	parameter for $\mathrm{Kir_{SMC}}$ opening rate, α_k	[3]
β_{KIR}	26.9 s	parameter for $\mathrm{Kir_{SMC}}$ closing rate, β_k	[3]
b_{v_1}	18 mV	parameter for $\mathrm{Kir_{SMC}}$ closing rate, β_k	[3]
b_{v_2}	0.06 mV	parameter for $\mathrm{Kir_{SMC}}$ closing rate, β_k	[3]

Table S5: Ω_{SMC} Vascular Smooth Muscle Cell Space

Ω_{SMC} Parameter		Source
Δ_P	60 mmHg	[28]
v_1	-23.265 mV	[17]
v_2	25 mV	[17]
v_4	14.5 mV	[17]
v_5	8 mV	[17]
v_6	-15 mV	[17]
Ca_3	400 nM	[17]
Ca_4	150 nM	[17]
ϕ_n	2.664	[17]
v_L	-70 mV	[17]
v_K	-85 mV	[17]
v_{Ca}	80 mV	[17]
C	19.635 pF	[17]
g_L	63.617 pS	[17]
g_K	314.16 pS	[17]
g_{Ca}	157 pS	[17]
K_d	1000 nM	[17]
B_T	10000 nM	[17]
α	4.3987e+15 nM C^{-1}	[17]
k_{Ca}	135.68 s^{-1}	[17]
Ca_m	170 nM	[17]
q	3	[17]
Ca_{ref}	285 nM	[17]
k_ψ	3.3	[17]
$\sigma^{\#}_{y_0}$	2.6e+06 dyne cm^{-2}	[17]
$\sigma^{\#}_0$	3e+06 dyne cm^{-2}	[17]
ψ_m	0.3	[17]

Ω_{SMC} Parameter		Source
ν_{ref}	0.24	[17]
a'	0.28125	[17]
b'	5	[17]
c'	0.03	[17]
d'	1.3	[17]
x'_1	1.2	[17]
x'_2	0.13	[17]
x'_3	2.2443	[17]
x'_4	0.71182	[17]
x'_5	0.8	[17]
x'_6	0.01	[17]
x'_7	0.32134	[17]
x'_8	0.88977	[17]
x'_9	0.0090463	[17]
u'_1	41.76	[17]
u'_2	0.047396	[17]
u'_3	0.0584	[17]
y'_0	0.928	[17]
y'_1	0.639	[17]
y'_2	0.35	[17]
y'_3	0.78847	[17]
y'_4	0.8	[17]
x_0	188.5 μm	[29]
a	753.98 μm^2	[30]
S	40000 μm^2	[30]
w_e	0.9	[17]
w_m	0.7	[17]
τ	0.2 dyne cm^{-1}	[17]

S4 Model Uncertainty

In this section, we address the uncertainty in the model by testing the effects of either omitting or modifying certain mechanisms of the model, as opposed to *parametric* uncertainty or parameter sensitivity analysis (Section S2, above, and Section 4 in the main paper).

S4.1 Astrocytic TRPV4 channels

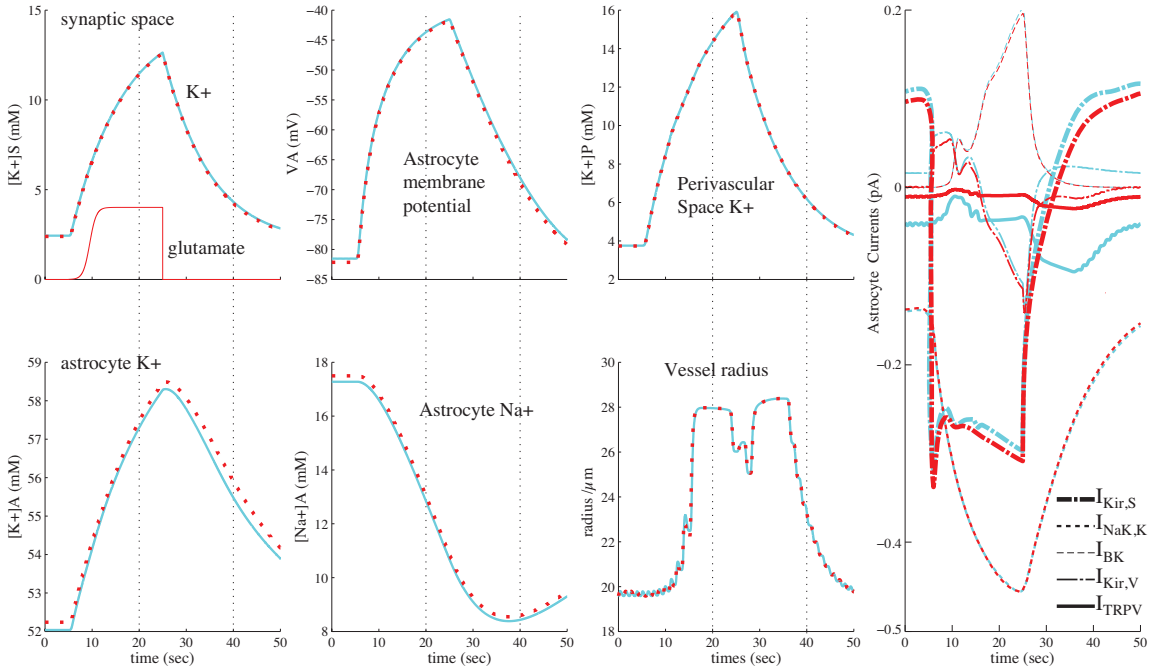

Figure S2: *Effects of TRPV4 K^+ and Na^+ effluxes.* Blue curves – original model from paper, in which TRPV4 includes only a Ca^{2+} permeability. Red curves – modified model in which TRPV4 current includes a Ca^{2+} influx as well as an outward K^+ and Na^+ component.

Because TRPV4 is a nonspecific cation channel, it is possible that it has a permeability to potassium and sodium ions [31]. In this model, we considered only the calcium component of the channel current, but we test here whether including potassium and sodium outward fluxes through astrocyte the TRPV4 channel would impact the neurovascular coupling in the simulation. Figure S2 compares the results from our model equations above (blue curves) with the results when we include K^+ and Na^+ TRPV4 currents. Because the data are limited on the specific K^+ and Na^+ permeabilities of astrocyte TRPV4, we estimate that the TRPV4 K^+ and Na^+ effluxes have equal magnitude and have a combined magnitude of 75% of the Ca^{2+} TRPV4 current. Based on our simulation results, the model is not particularly sensitive to the addition of the TRPV4 K^+ and Na^+ effluxes, as the astrocyte Kir channels, particularly at the endfoot, oppose the hyperpolarizing effects of the TRPV4 effluxes. Also, because the Kir channels are sensitive to extracellular K^+, the TRPV4 potassium efflux into the perivascular space causes a reduction in the endfoot Kir potassium release, leaving the perivascular potassium almost unchanged after adding K^+ and Na^+ effluxes to the TRPV4 model. Because of the limited data on TRPV4 K^+ and Na^+ currents and the low sensitivity of such currents in our model, we find that it is preferable to leave these out of the model, although they can be added in the future as more data are available.

S4.2 Timing of vascular response onset

In our previous paper [16], we made a correction for the time delay in the onset of vessel dilation by adjusting the Kir_{SMC} parameters. However, in this paper, we found that including astrocyte Kir channels provides a faster K^+ release mechanism from the astrocyte endfoot, thereby speeding the vessel response time by increasing perivascular potassium earlier. In Figure S3, we compare the effects of these two different "fixes."

The red curves show the results when we remove the astrocytic Kir_{AS} and Kir_{AV} from the model as in Section 3.1.1 of the main paper (see $\overline{I_{AS}}$) and we adjust the arteriole Kir_{SMC} parameters to improve the speed of the vessel response. The simulation for red curves is thus analogous to the that of our previous paper, in which the astrocyte

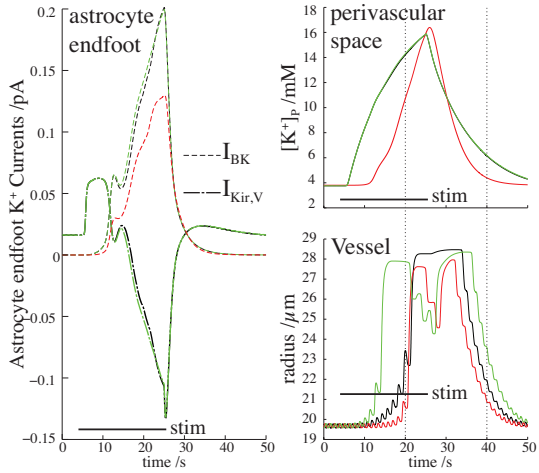

Figure S3: Left – astrocyte BK and Kir_{AV} currents. Top right – perivascular K^+. Bottom right – arteriole radius. Black bars indicate time of neural stimulus. Black curves – unadjusted Kir_{SMC} parameters; astrocyte Kir and BK currents. Red curve – adjusted Kir_{SMC} parameters, astrocyte model Kir currents excluded (see $\overline{I_{AS}}$ in Section 3.1.1 of the main paper). Green curve – inclusion of both fixes, Kir_{SMC} parameter adjustments and astrocytic Kir channels. Including both fixes does not reduce delay in the response onset, but it dramatically increases the initial speed of the dilation. The the Kir_{SMC} parameter adjustment is necessary for the vessel to constrict at >15 mM K^+, the Kir_{SMC} (green and red curves). The secondary dilation shown in these two curves occurs after the extracellular K^+ has begun its decrease, at which point, the vessel response initially favors dilation while the K^+ is still moderately high (∼8-14 mM)

model did not include Kir channels. The black curves are the results when astrocytic Kir currents are included, but there is no adjustment to the arteriole Kir_{SMC} parameters. In the plot for vessel radius vs. time (bottom right), note that although the black and red curves reach their peak values at about the same time, the black curve begins its rise several seconds earlier and initially increases at a faster rate. In addition, the red curve shows that the vessel reconstricts at a lower extracellular potassium concentration than what would be required for the black curve. The results when including both fixes are shown in the green curves: the parameters for arteriole Kir_{SMC} are the same for the green curves as for the red curves, but the astrocyte $\text{Kir}_{AS/AV}$ currents are also included. The result is that the vessel begins its dilation response at about the same time as the black curve, but at a faster rate, and it reaches its peak dilation 8-10 seconds earlier, and the vessel also reconstricts when the perivascular potassium (top right) exceeds roughly 14 mM.

The physiological rationale for including the Kir_{SMC} parameter adjustments is that they allow the vessel to respond appropriately to the level of extracellular K^+. The original parameter values used by [3] give reasonable results for higher extracellular potassium levels (10 mM and above), but they leave the vessel less sensitive to more moderate rises in extracellular potassium (4-9 mM), which is not physiologically accurate (Fig. 3 in [3] illustrates this). An overcorrection would occur if the Kir_{SMC} parameters were adjusted enough that the vessel began to respond with dilations for inappropriately low extracellular K^+.

S4.3 Role of astrocyte BK channels on neurovascular coupling

In this section we consider the effect of astrocytic endfoot BK channels on neurovascular coupling. Figure S4 shows the results from our model when the astrocyte BK channels are omitted. The top plot shows the perivascular

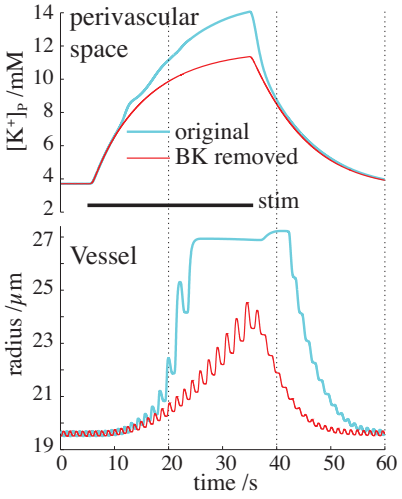

Figure S4: Astrocyte BK channel effect on neurovascular coupling. A 30 second neural stimulus occurs starting at time = 5 seconds (black horizontal bar). Blue curves – results under control conditions (with BK channels, as in main paper). Red curves – results when astrocytic BK channels are removed by setting the astrocyte Top plot – perivascular potassium concentration. Bottom plot – arteriole radius. BK conductance to 0.

potassium concentration during a 30 second neural stimulus (indicated by the black, horizontal bar), and the bottom plot shows the vessel radius. The blue curves are the results when the model is unchanged from the equations in the

main paper, and the red curves are the results when we remove the BK channels from the astrocyte model. Although the astrocyte Kir can sustain a moderate potassium efflux, without the BK channels, the perivascular potassium, and consequentially the vessel dilation, is significantly reduced according to our model.

These results seem reasonable based on the literature. A study by [32] found that the BK channel blockers paxilline and TEA inhibited astrocyte mGluR-induced outward current, which was reduced by 87.6%. Similarly, [24] found that BK channels in astrocyte endfeet produced large-conductance outward potassium currents that were activated by neural stimulation, and that blocking BK channels or ablating the gene encoding BK channels actually prevented neuronally induced vasodilation, which is believed to be caused by astrocyte release of potassium at the gliovascular space. Another study demonstrated that *rSlo* K_{Ca} (BK) channels are highly concentrated in astrocyte perivascular endfeet [33].

S4.4 Adult brain astrocyte model

Recent experimental work by [34] demonstrates a fundamental difference between astrocyte glutamate receptor expression in young and adult brains, suggesting the possibility that only astrocytes from young brains respond to synaptic glutamate release with an intracellular calcium rise. The glutamate receptor linked to IP_3 production and

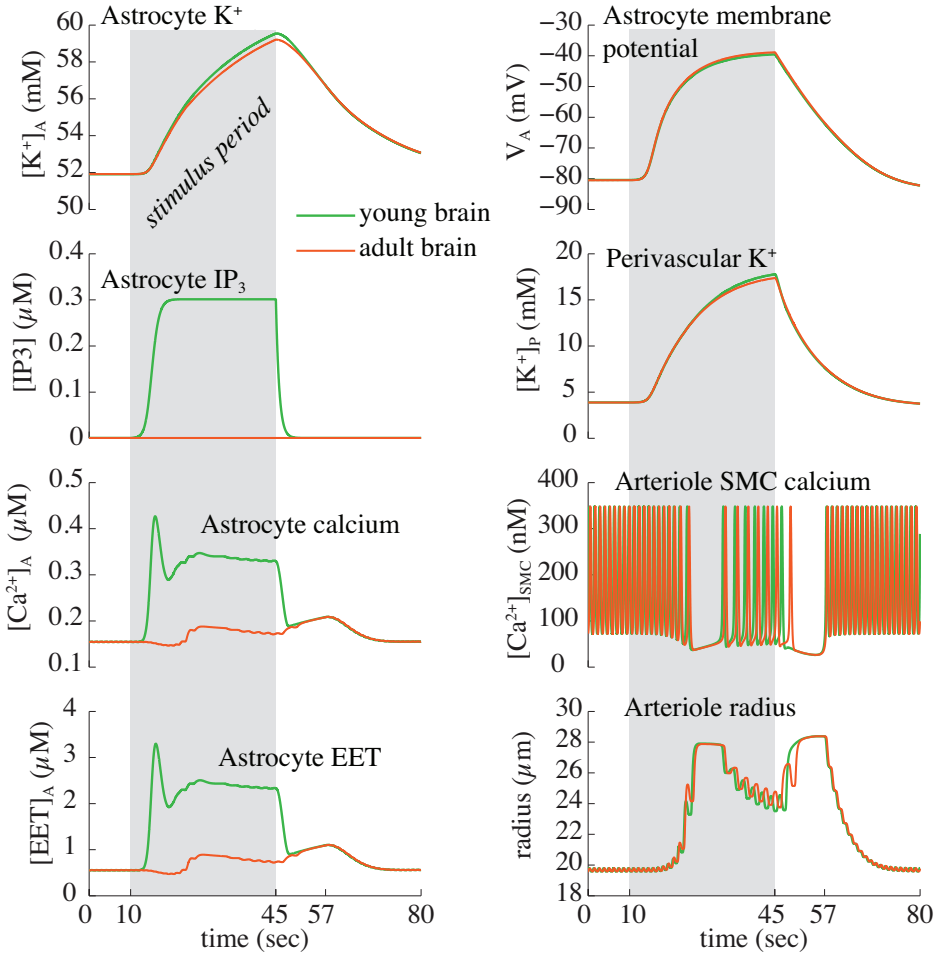

Figure S5: Comparison of young and "adult brain" astrocyte models. Green lines are the young brain model; red lines are the modified "adult" brain model. Shaded area indicates time period of neural stimulus

subsequent intracellular Ca^{2+} increase is mGluR5; the results in [34] show that cortical astrocytes from developing brains expressed mGluR5, but that both adult human and adult mouse cortical astrocytes did not. The same study found that the primary type of mGluR expressed in adult cortical astrocytes is mGluR3, which does not trigger Ca^{2+} increases.

Based on these findings we explore a possible preliminary model of an adult brain astrocyte which is a modified version of the main equations above. In the modified "adult" version of the model, we remove the glutamate triggered IP_3/Ca^{2+}/EET pathway (removing Eq. (S3) and setting $J_{IP_3} = 0$ in Eq. (S12)) that is characteristic of the mGluR5, but not mGluR3.

Results comparing the original young brain model and the modified "adult" brain model are shown in Figure S5. The green curves are from the original model, and the red curves are the results from the adult brain model. What is

interesting is that the that neural-induced vasodilation is predicted in both the young brain model and the modified "adult" model, suggesting that the astrocyte glutamate receptors may play a smaller role than expected in functional hyperemia. In fact, the modeling paper by [3] suggested that the intracellular calcium and EET rises due to astrocyte mGluR activation were necessary for vasodilation because calcium and EET both activate the BK potassium outflux at the astrocyte perivascular endfeet. They propose that astrocytic potassium "is released by endfoot BK channels due to the action of EETs on them, not due to the depolarising membrane." Upon experimenting with the equations from their paper, we found that what they propose is true for the small astrocyte depolarizations simulated in their paper. However, when we increased the amplitude of the neuronal potassium release, we found that the resulting increase in astrocyte depolarization was sufficient to activate the astrocyte BK channels even when glutamate was excluded from the simulation. Our model prediction that astrocyte-mediated neural induced vasodilation does not depend on astrocyte mGluR activity could potentially be a unifying property of astrocytes in developing and mature brains; the functional differences may have more to do with IP_3 and Ca^{2+} dependent glutamate release from astrocytes which would occur in developing brains, but not in mature brains, whose astrocytes lack mGluR5. This difference could potentially be related to what distinguishes learning in the developing and adult brains.

We also note that the above findings contradict the ideas proposed by [35]. While we recognize the importance of the work, we are cautious about dismissing astrocyte spatial potassium transfer altogether as a mechanism for neurovascular coupling. First, the experiments in [35] were performed in the retina, which is a unique and very distinctive part of the brain, and the types of astrocytes expressed in the retina are primarily fibrous, a functionally and biochemically different class from the protoplasmic astrocytes typically found in the cortex. Second, the implications of the study are slightly unclear: the authors state that astrocyte endfeet release potassium in response to depolarization. The authors also demonstrate that application of extracellular potassium near an arteriole induces a dilation. However, the paper does not focus on addressing the reason why depolarizing an astrocyte in contact with an arteriole might still fail to produce a dilation. In other words, if depolarized astrocytes release potassium from their vessel-adjacent endfeet, and if application of potassium alone dilates vessels, then why would it be that astrocyte depolarization does not dilate vessels? It seems the only possible implication is that the astrocyte does not release sufficient amounts of potassium, but the authors state in the discussion that the current injection in the experiment was large enough and localized properly on the astrocyte "ensuring that the experimentally produced depolarizations will evoke significant K^+ efflux from the endfeet." One thing that the authors do not discuss is the initial arteriole tone: if an arteriole is in or near its fully dilated state, neural stimulation or application of potassium would not cause a dilation at all (see [36]).

Supporting References

[1] Koenigsberger, M., R. Sauser, J.-L. Bény, and J.-J. Meister. 2006. Effects of arterial wall stress on vasomotion. *Biophysical Journal*. 91:1663–1674.

[2] Bennett, M. R., L. Farnell, and W. Gibson. 2008. Origins of blood volume change due to glutamatergic synaptic activity at astrocytes abutting on arteriolar smooth muscle cells. *Journal of Theoretical Biology*. 250:172–185.

[3] Farr, H., and T. David. 2011. Models of neurovascular coupling via potassium and EET signalling. *Journal of Theoretical Biology*. 286:13–23.

[4] Østby, I., L. Øyehaug, G. T. Einevoll, E. A. Nagelhus, E. Plahte, T. Zeuthen, C. M. Lloyd, O. P. Ottersen, and S. W. Omholt. 2009. Astrocytic mechanisms explaining neural-activity-induced shrinkage of extraneuronal space. *PLoS Computational Biology*. 5:e1000272.

[5] Hibino, H., A. Inanobe, K. Furutani, S. Murakami, I. Findlay, and Y. Kurachi. 2010. Inwardly rectifying potassium channels: their structure, function, and physiological roles. *Physiological Reviews*. 90:291–366.

[6] Kofuji, P., B. Biedermann, V. Siddharthan, M. Raap, I. Iandiev, I. Milenkovic, A. Thomzig, R. Veh, A. Bringmann, and A. Reichenbach. 2002. Kir potassium channel subunit expression in retinal glial cells: Implications for spatial potassium buffering. *Glia*. 39:292–303.

[7] Ishii, M., A. Fujita, K. Iwai, S. Kusaka, K. Higashi, A. Inanobe, H. Hibino, and Y. Kurachi. 2003. Differential expression and distribution of kir5. 1 and kir4. 1 inwardly rectifying k+ channels in retina. *American Journal of Physiology-Cell Physiology*. 285:C260–C267.

[8] Higashimori, H., and H. Sontheimer. 2007. Role of Kir4. 1 channels in growth control of glia. *Glia*. 55:1668–1679.

[9] Odette, L. L., and E. A. Newman. 1988. Model of potassium dynamics in the central nervous system. *Glia*. 1:198–210.

[10] Nilius, B., J. Vriens, J. Prenen, G. Droogmans, and T. Voets. 2004. TRPV4 calcium entry channel: a paradigm for gating diversity. *American Journal of Physiology Cell Physiology*. 286:C195–C205.

[11] Watanabe, H., J. Vriens, A. Janssens, R. Wondergem, G. Droogmans, and B. Nilius. 2003. Modulation of TRPV4 gating by intra- and extracellular Ca^{2+}. *Cell Calcium*. 33:489–495.

[12] Hamill, O. P., and B. Martinac. 2001. Molecular basis of mechanotransduction in living cells. *Physiological Review*. 81:685–733.

[13] Nilius, B., H. Watanabe, and J. Vriens. 2003. The TRPV4 channel: structure-function relationship and promiscuous gating behaviour. *European Journal of Physiology*. 446:298–303.

[14] Strotmann, R., G. Schultz, and T. D. Plant. 2003. Ca^{2+}-dependent potentiation of the nonselective cation channel TRPV4 is mediated by a C-terminal calmodulin binding site. *Journal of Biological Chemistry*. 278:26541–26549.

[15] Fernandes, J., I. M. Lorenzo, Y. N. Andrade, A. Garcia-Elias, S. A. Serra, J. M. Fernández-Fernández, and M. A. Valverde. 2008. IP3 sensitizes TRPV4 channel to the mechano-and osmotransducing messenger 5'-6'-epoxyeicosatrienoic acid. *Journal of Cell Biology*. 181:143–155.

[16] Witthoft, A., and G. E. Karniadakis. 2012. A bidirectional model for communication in the neurovascular unit. *Journal of Theoretical Biology*. 311:80–93.

[17] Gonzalez-Fernandez, J. M., and B. Ermentrout. 1994. On the origin and dynamics of the vasomotion of small arteries. *Mathematical Biosciences*. 119:127–167.

[18] Haddock, R., G. Hirst, and C. Hill. 2002. Voltage independence of vasomotion in isolated irideal arterioles of the rat. *The Journal of Physiology*. 540:219–229.

[19] Hudetz, A. G., K. A. Conger, J. H. Halsey, M. Pal, O. Dohan, and A. G. B. Kovach. 1987. Pressure distribution in the pial arterial system of rats based on morphometric data and mathematical models. *Journal of Cerebral Blood Flow & Metabolism*. 7:342–355.

[20] Smolyak, S. 1963. Quadrature and interpolation formulas for tensor products of certain classes of functions. *In* Dokl. Akad. Nauk SSSR, volume 4. 240–243.

[21] Sobol, I. M. 2001. Global sensitivity indices for nonlinear mathematical models and their Monte Carlo estimates. *Mathematics and Computers in Simulation*. 55:271–280.

[22] Heiss, F., and V. Winschel. 2006. Estimation with numerical integration on sparse grids. Department of Economics Discussion paper 2006-15, University of Munich, http://econpapers.repec.org/paper/lmumuenec/916.htm.

[23] Parthimos, D., D. H. Edwards, and T. M. Griffith. 1999. Minimal model of arterial chaos generated by coupled intracellular and membrane Ca^{2+} oscillators. *American Journal of Physiology-Heart and Circulatory Physiology*. 277:H1119–H1144.

[24] Filosa, J. A., A. D. Bonev, S. V. Straub, A. L. Meredith, M. K. Wilkerson, R. W. Aldrich, and M. T. Nelson. 2006. Local potassium signaling couples neuronal activity to vasodilation in the brain. *Nature Neuroscience*. 9:1397–1403.

[25] Kung, C. 2005. A possible unifying principle for mechanosensation. *Nature*. 436:647–654.

[26] Benfenati, V., M. Amiry-Moghaddam, M. Caprini, M. N. Mylonakou, C. Rapisarda, O. P. Ottersen, and S. Ferroni. 2007. Expression and functional characterization of transient receptor potential vanilloid-related channel 4 (TRPV4) in rat cortical astrocytes. *Neuroscience*. 148:876–892.

[27] Cao, R. 2011. The hemo-neural hypothesis: Effects of vasodilation on astrocytes in mammalian neocortex. Ph.D. thesis, Department of Brain & Cognitive Sciences, Massachusetts Institute of Technology, Cambridge, Massachusetts.

[28] Horiuchi, T., H. H. Dietrich, K. Hongo, and R. G. Dacey. 2002. Mechanism of extracellular K^+-induced local and conducted responses in cerebral penetrating arterioles. *Stroke*. 33:2692–2699.

[29] Ngai, A. C., and H. R. Winn. 1995. Modulation of cerebral arteriolar diameter by intraluminal flow and pressure. *Circulation Research*. 77:832–840.

[30] Dacey, R. G., Jr., and B. R. Duling. 1982. A study of rat intracerebral arterioles: methods, morphology, and reactivity. *American Journal of Physiology*. 243:H598–H606.

[31] Taniguchi, J., S. Tsuruoka, A. Mizuno, J.-i. Sato, A. Fujimura, and M. Suzuki. 2007. TRPV4 as a flow sensor in flow-dependent K^+ secretion from the cortical collecting duct. *American Journal of Physiology-Renal Physiology*. 292:F667–F673.

[32] Higashimori, H., V. Blanco, V. Tuniki, J. Falck, and J. Filosa. 2010. Role of epoxyeicosatrienoic acids as autocrine metabolites in glutamate-mediated K^+ signaling in perivascular astrocytes. *American Journal of Physiology-Cell Physiology*. 299:C1068–C1078.

[33] Price, D. L., J. W. Ludwig, H. Mi, T. L. Schwarz, and M. H. Ellisman. 2002. Distribution of rSlo Ca^{2+}-activated K^+ channels in rat astrocyte perivascular endfeet. *Brain Research*. 956:183 – 193.

[34] Sun, W., E. McConnell, J.-F. Pare, Q. Xu, M. Chen, W. Peng, D. Lovatt, X. Han, Y. Smith, and M. Nedergaard. 2013. Glutamate-dependent neuroglial calcium signaling differs between young and adult brain. *Science*. 339:197–200.

[35] Metea, M. R., P. Kofuji, and E. A. Newman. 2007. Neurovascular coupling is not mediated by potassium siphoning from glial cells. *The Journal of Neuroscience*. 27:2468–2471.

[36] Blanco, V. M., J. E. Stern, and J. A. Filosa. 2008. Tone-dependent vascular responses to astrocyte-derived signals. *American Journal of Physiology-Heart and Circulatory Physiology*. 294:H2855–H2863.